Electronic Transactions on Numerical Analysis.
Volume 61, pp. 173–195, 2024.

ISSN 1068–9613.
DOI: 10.1553/etna_vol61s173

ETNA
Kent State University and
Johann Radon Institute (RICAM)

LINEAR FDEM SUBSOIL DATA INVERSION IN BANACH SPACES*

P. DÍAZ DE ALBA†, C. ESTATICO‡, M. LAZZARETTI‡, AND G. RODRIGUEZ§

Dedicated to Giuseppe Rodriguez on the occasion of his 60th birthday.

Abstract. The applicative motivation of this paper is the reconstruction of some electromagnetic features of the earth superficial layer by measurements taken above the ground. We resort to frequency domain electromagnetic data inversion through a well-known linear integral model by considering three different collocation methods to approximate the solution of the continuous problem as a linear combination of linearly independent functions. The discretization leads to a strongly ill-conditioned linear system. To overcome this difficulty, an iterative regularization method based on Landweber iterations in Banach spaces is applied to reconstruct solutions which present discontinuities or have a low degree of smoothness. This kind of solutions are common in many imaging applications. Several numerical experiments show the good performance of the algorithm in comparison to other regularization techniques.

Key words. first-kind Fredholm integral equations, electromagnetic induction, inverse problems in geophysics, collocation methods, iterative regularization, Landweber method, Banach spaces

AMS subject classifications. 45B05, 65F22, 65R20, 86A22

1. Introduction.

We are interested in reconstructing the electrical conductivity profile of the subsoil as a function of depth by inverting electromagnetic induction (EMI) data. Frequency domain electromagnetic data (FDEM) is a very useful prospection method in applied Geophysics, as it provides information about underground conductive materials, like pollutants, saline water, or unexplored ordnance, by a relatively simple instrumentation.

There exists different mathematical models (linear and nonlinear) to describe the interaction between the soil and the electromagnetic field generated by the instrument. A typical approach is to solve the inverse problem for such models to obtain a physically significant solution. Here, we focus our attention on the linear integral model first introduced in [35], which is composed by two Fredholm integral equations of the first kind, each one corresponding to a particular configuration of the measuring device; we refer to Section 2 for a detailed description of the model.

When dealing with low induction numbers, i.e., low values of the electrical conductivity, this linear integral model is accurate enough to yield acceptable reconstructions. Quite recently, some authors have analyzed this model from both the theoretical and the numerical points of view; see [22, 23]. In [23], the continuous problem has been studied in various function spaces and three different collocation methods have been proposed to discretize the problem. After applying a particular procedure to deal with the integral truncation error, an ill-conditioned linear system was obtained. The resulting systems of equations have different structures, but there are no significant differences in their conditioning, so some regularization techniques based on the truncated singular value (TSVD) and the truncated generalized SVD (TGSVD) decompositions were considered. A different approach was proposed in [22], where a regularized minimal-norm solution was computed in a reproducing kernel Hilbert space, under the assumption that boundary constraints are available.

*Received June 20, 2024. Accepted November 21, 2024. Published online on February 4, 2025. Recommended by A. Buccini.
†Department of Mathematics, University of Salerno, via Giovanni Paolo II 132, 84084 Fisciano (SA), Italy (pdiazdealba@unisa.it).
‡Department of Mathematics, University of Genoa, via Dodecaneso 35, 16146 Genoa, Italy ({estatico,lazzaretti}@dima.unige.it).
§Department of Mathematics and Computer Science, University of Cagliari, via Ospedale 72, 09124 Cagliari, Italy (rodriguez@unica.it).

ETNA
Kent State University and
Johann Radon Institute (RICAM)

It is important to note that for high conductivity values, the linear model does not accurately represent the physics of the problem. In such cases, a nonlinear approach is preferable, as it provides a greater accuracy. Different numerical techniques for the analysis of such a nonlinear model have been studied in [10, 18, 19, 20, 21, 38, 39], and a Matlab toolbox implementing the algorithms introduced in the papers has been released [16, 17]. Since the solution of a nonlinear problem typically reduces to the solution of a sequence of linear problems, the techniques explored in this paper may be relevant also in the nonlinear setting, as they would influence the choice of a regularized solution. This will the subject of future work.

Fredholm integral equations of the first kind are in general ill-posed problems, hence they lead to strongly ill-conditioned linear systems, so regularization methods are of primary importance for their solution. A typical regularization technique for this kind of problems consists of imposing smoothness constraints on the solution. However, this is not always the best approach in specific applications where sharp interfaces might be present. This may happen in our problem for a stratified soil or in the presence of buried archaeological remains, since such scenario would produce a discontinuous distribution of the electrical conductivity. In these situations, approximating a piecewise constant profile by a smooth solution may produce inaccurate results or even a misleading outcome. For such situations, it is interesting to employ regularization methods which promote discontinuities in the solution.

Classical regularization methods in Hilbert spaces are based on the spectral decomposition of the linear operator to be inverted. The analysis of single eigencomponents gives useful information about the convergence of the methods and their regularization properties. Anyway, the spectral-based methods, in general, lead to smooth (and sometimes over-smooth) solutions. This becomes an important disadvantage in practical applications where a non-smooth behavior of the solution arises. Indeed, in many geophysical prospection scenarios a smoothly varying dielectric distribution is rarely encountered, because strong boundaries between essentially homogeneous but different materials occur.

In order to obtain physically relevant reconstructions of non-smooth solutions for ill-posed inverse problems, Banach spaces have been considered to introduce and investigate regularization methods; see [41]. Such spaces are complete vector spaces endowed with a norm that allows "lengths" and "distances" between its elements to be measured, without an inner product which induces the norm.

Some of the advantages of these methods are the following: 1) They have geometrical properties such that the associated solutions are endowed with less over-smoothness. This results, for instance, in a better localization and restoration of the discontinuities or localized impulsive signals in imaging applications. 2) They produce sparse solutions, in the sense that they can be represented by few coefficients in an appropriate basis; see [6, 41]. This is very useful when dealing with large-scale problems, where sparsity yields low complexity in computation and storage. We point out that sparsity in Banach spaces is a fast emerging research field, with a lot of real applications in learning theory and compressed sensing [42, 43].

In this work, attention is focused on the inversion of FDEM data by combining the different collocation methods discussed in [23] to the regularization techniques in Banach spaces discussed in [41]. The new results are compared to those obtained in [23] by applying the TSVD and the TGSVD as regularization methods.

The paper is organized as follows: Section 2 starts with a description of the linear integral model based on a particular device used to collect FDEM data, while in Section 3 we review three different collocation methods which lead to the linear system to be solved. In order to describe the proposed iterative regularization method, a brief introduction to Banach spaces is provided in Section 4, and Section 5 presents the numerical regularization procedure which

ETNA
Kent State University and
Johann Radon Institute (RICAM)

we propose to apply to the FDEM problem. Numerical examples that show the efficiency of the whole algorithm are presented in Section 6, and some conclusions and future work are reported in Section 7.

2. The linear EM model. A well-known device for frequency domain electromagnetic (FDEM) geophysical prospection is a ground conductivity meter. Its transmitter coil generates a primary electromagnetic field at a fixed frequency f that propagates in the ground. Conductors present in the under soil, when crossed by the EM field, produce a secondary field by electromagnetic induction. This field is measured by the receiver coil, placed at a fixed distance ρ from the transmitter. The coils can be aligned in various positions, here we just consider vertical (V) and horizontal (H) magnetic dipoles.

A mathematical model for FDEM prospection was introduced in [35] for the Geonics EM-38 device ($f = 14300$Hz, $\rho = 1$m), assuming a linear dependence between the instrument response and the region of soil beneath the ground level. The model is composed by two Fredholm integral equations of the first kind, corresponding to the V- and H-orientations of the device, respectively. It reads

$$\begin{cases} \displaystyle\int_0^\infty k^V(z+h)\,\sigma(z)\,dz = b^V(h), \\ \displaystyle\int_0^\infty k^H(z+h)\,\sigma(z)\,dz = b^H(h), \end{cases} \tag{2.1}$$

where the kernels k^V and k^H are defined by

$$k^V(z) = \frac{4z}{(4z^2+1)^{3/2}}, \qquad k^H(z) = 2 - \frac{4z}{(4z^2+1)^{1/2}},$$

and $\sigma(z)$ represents the value of the electrical conductivity, expressed in Siemens/meter (S/m), at depth $z\rho$ below the ground surface. The right-hand sides $b^V(h)$ and $b^H(h)$ stand for the readings of the instrument (usually considered as the *apparent conductivity* of the soil) at height $h\rho > 0$ above the ground, for the two possible orientations. We remark that the variables z and h are variables that indicate the depth and height as a multiple of the intercoil distance ρ.

REMARK 2.1. The linear model prediction is considered reliable when the conductivity of the area under investigation is relatively low, i.e., $\sigma \simeq 0.1$ S/m. In the case where the conductivity values are expected to be larger, a nonlinear model is available and has been studied by many authors; see, e.g., [10, 17, 18, 19, 21, 23].

3. Discretization of the forward problem. Following [23], the forward model is discretized by expressing the electrical conductivity $\sigma(z)$ as a linear combination of linearly independent functions $\varphi_j(z)$ with coefficients c_j, for $j = 1, 2, \ldots$, that is,

$$\sigma(z) \simeq \sum_{j=1}^{\infty} c_j \varphi_j(z). \tag{3.1}$$

A collocation method is employed by evaluating the right-hand sides at different heights $h_1, h_2, \ldots, h_m$ above the ground, so that model (2.1) becomes

$$\begin{cases} \displaystyle\sum_{j=1}^{\infty} c_j \int_0^\infty k^V(z+h_i)\varphi_j(z)\,dz = b^V(h_i), \\ \displaystyle\sum_{j=1}^{\infty} c_j \int_0^\infty k^H(z+h_i)\varphi_j(z)\,dz = b^H(h_i), \end{cases} \tag{3.2}$$

ETNA
Kent State University and
Johann Radon Institute (RICAM)

for $i = 1, \dots, m$.

In [23], a particular truncation of the sums involved in (3.2) was introduced. We report it here briefly. The integrals appearing in (2.1) are split as follows:

$$\int_0^\infty k^V(h+z)\sigma(z)\,dz = \int_0^\tau k^V(h+z)\sigma(z)\,dz + \int_\tau^\infty k^V(h+z)\sigma(z)\,dz,$$
$$\int_0^\infty k^H(h+z)\sigma(z)\,dz = \int_0^\tau k^H(h+z)\sigma(z)\,dz + \int_\tau^\infty k^H(h+z)\sigma(z)\,dz,$$

for some $\tau > 0$. Moreover, the kernels k^V and k^H are continuous and integrable functions,

$$k^V(z) = \frac{d}{dz}\left(-\frac{1}{\sqrt{4z^2+1}}\right), \qquad k^H(z) = \frac{d}{dz}\left(2z - \sqrt{4z^2+1}\right).$$

They are known as *sensitivity functions*, since they reflect the relative contribution of the electrical conductivity to the secondary EM field at depth $z\rho$. Indeed, in the V-orientation, the device is most sensitive around $z = \sqrt{2}/4$, while in the H-orientation, it is most sensitive near the surface and the sensitivity rapidly decays for increasing depth.

Assuming $\sigma(z) \le C$, for $z \ge \tilde{z}$, where $\tilde{z}$ is either 0 or a rough underestimate of τ, we have the following upper bound for the equations:

$$\int_\tau^\infty k^V(h+z)\sigma(z)\,dz \le C\int_\tau^\infty k^V(h+z)\,dz = CR_V(h),$$
$$\int_\tau^\infty k^H(h+z)\sigma(z)\,dz \le C\int_\tau^\infty k^H(h+z)\,dz = CR_H(h),$$

with

$$R_V(h) = \frac{1}{\sqrt{4(h+\tau)^2+1}}, \qquad R_H(h) = \sqrt{4(h+\tau)^2+1} - 2(h+\tau).$$

By requiring that both quantities are smaller than a given tolerance ϵ for any $h \ge 0$, we obtain that the truncation parameter τ must be chosen larger than $C(2\epsilon)^{-1}$. The bound C may often be estimated by a priori information on the composition of deep layers of the undersoil under scrutiny.

On the one hand, physical considerations suggest that the sensitivity of the measuring device is limited to the depth range $[0, a\rho]$, with $a \simeq 3$–4, so taking $\tau \gg a$ would lead to an unnecessarily large linear system. On the other hand, once τ is chosen, the series in (3.2) can be truncated to a finite number of terms, corresponding to writing the conductivity as

$$\sigma(z) \simeq \sum_{j=1}^{n} c_j \varphi_j(z). \tag{3.3}$$

So τ and n will be related through the localization of the basis elements φ_j.

Thus, the above discussed discretization leads to the linear system

$$F\mathbf{c} = \mathbf{g}, \tag{3.4}$$

where $F \in \mathbb{R}^{2m\times n}$ has entries

$$f_{ij} = \begin{cases} \displaystyle\int_0^\tau k^V(z+h_i)\varphi_j(z)\,dz, & i = 1, \dots, m, \\ \displaystyle\int_0^\tau k^H(z+h_{i-m})\varphi_j(z)\,dz, & i = m+1, \dots, 2m, \end{cases} \tag{3.5}$$

ETNA
Kent State University and
Johann Radon Institute (RICAM)

with $j = 1, \ldots, n$, and the components of $\mathbf{g} \in \mathbb{R}^{2m}$ are given by

$$g_i = \begin{cases} b^V(h_i) - CR_V(h_i), & i = 1, \ldots, m, \\ b^H(h_{i-m}) - CR_H(h_{i-m}), & i = m+1, \ldots, 2m. \end{cases}$$

By solving (3.4), one obtains the coefficient vector $\mathbf{c} = (c_1, \ldots, c_n)^T$ needed to construct the numerical approximation (3.1) of the solution.

We remark here that problem (2.1), being composed by Fredholm integral equations of the first kind, leads to an ill-posed problem in the sense of Hadamard [28], namely, a problem that may have no solutions in a desired class, may admit infinitely many solutions, or is such that a small perturbation in the data may lead to arbitrarily large errors in the solution; this point has been discussed in [23], where conditions for well-posedness have been described.

This fact makes system (3.4) severely ill-conditioned. It is then necessary to resort to suitable regularization techniques to solve it with a reasonable accuracy. In this paper we propose an iterative regularization method in Banach spaces; see Section 5.

In [23], three different choices for the functions φ_j have been analyzed to approximate the solution. In the following, we briefly review the corresponding collocation procedures which lead to the construction of the coefficient matrix F in (3.4).

3.1. Piecewise constant functions. As a first choice, we use piecewise constant functions, or B-splines of order 1, (see [15, 30]) for the approximation of the solution in (3.1), that is,

$$\varphi_j(z) = \begin{cases} 1, & z_{j-1} \le z < z_j, \\ 0, & \text{otherwise}, \end{cases} \tag{3.6}$$

with $j = 1, \ldots, n$, so that $z_0 = 0$ and $z_n = \tau$.

By replacing (3.3) in (2.1) and collocating each equation at different measurements heights h_i, $i = 1, \ldots, m$, we obtain system (3.2) with a finite number n of terms in the sums. From definitions (3.5) and (3.6), an explicit form for the entries of F in the system (3.4) can be found. They are reported in [23, Section 3.1].

REMARK 3.1. Note that the exact solution vector of both equations in the system (2.1) is the same. So, one may think of solving the linear system corresponding to only one orientation of the device. We stress that, given the ill-conditioning of the system and the presence of experimental errors in the right-hand side, solving the overdetermined linear system corresponding to both orientations in the least-squares sense generally gives more accurate results, as it uses the largest amount of available information to solve the inverse problem.

3.2. Linear splines. In this case, in the approximation (3.3) we use linear splines, i.e., B-splines of order 2 [15, 30], in the form

$$\varphi_0(z) = \begin{cases} \dfrac{1}{\delta_1}(z_1 - z), & z_0 \le z < z_1, \\ 0, & \text{otherwise}, \end{cases}$$

and

$$\varphi_j(z) = \begin{cases} \dfrac{1}{\delta_j}(z - z_{j-1}), & z_{j-1} \le z < z_j, \\ \dfrac{1}{\delta_{j+1}}(z_{j+1} - z), & z_j \le z < z_{j+1}, \\ 0, & \text{otherwise}, \end{cases}$$

ETNA
Kent State University and
Johann Radon Institute (RICAM)

for $j = 1, 2, \ldots, n$, with $\delta_j = z_j - z_{j-1}$.

Following the same procedure as in Section 3.1, closed formulae for the entries of the linear system were obtained in [23, Section 3.2].

REMARK 3.2. In the case of a uniformly spaced discretization, it is easy to see that, in this case and in the previous one, the coefficient matrix F is composed of two blocks that are Hankel matrices, except for their first columns; see [23].

3.3. Bernstein polynomials. The third collocation scheme is based on Bernstein polynomials. By introducing the change of variable $z = \tau y$ in (2.1), the integrand is approximated by a Bernstein polynomial

$$k^{V,H}(\tau y + h)\sigma(\tau y) = \sum_{j=0}^{n} k^{V,H}(\tau y_j + h)\sigma(\tau y_j)\, p_{nj}(y),$$

where $y_j = z_j/\tau$, $j = 0, 1, \ldots, n$, and

$$p_{nj}(z) = \binom{n}{j} z^j (1-z)^{n-j}.$$

Collocating the resulting equation at the heights h_i, $i = 1, \ldots, m$, the analytic expression of the entries of the matrix F in (3.4) is easily found. A detailed description can be found in [23].

4. Mathematics background of Banach spaces. Before discussing an iterative method for solving problem (3.4), we first sketch basic tools and notations of regularization in Banach spaces, including duality mappings and Bregman distances [13, 34, 41].

Let $\mathcal{X}$ and $\mathcal{Y}$ be two real Banach spaces, that is, two normed vector spaces that are complete with respect to the metric induced by each corresponding norm. We recall that, differently from Hilbert spaces, no scalar product is in general defined in a Banach space, so that the conventional concepts of "angle" and "orthogonality" between elements are not defined. As usual $\mathcal{X}^*$ denotes the dual space of $\mathcal{X}$, that is, the Banach space of all bounded linear functionals $x^* : \mathcal{X} \longrightarrow \mathbb{R}$, equipped with the norm [8]

$$\|x^*\|_{\mathcal{X}^*} = \sup_{\|x\|=1} |x^*(x)|.$$

Throughout the paper, we omit subscripts indicating the space when implicitly clear.

For any $x^* \in \mathcal{X}^*$ and $x \in \mathcal{X}$, both the duality pairings $\langle x^*, x\rangle$ and $\langle x, x^*\rangle$ represent the action of the linear functional x^* on the element x, that is

$$\langle x^*, x\rangle_{\mathcal{X}^*\times\mathcal{X}} = \langle x, x^*\rangle_{\mathcal{X}\times\mathcal{X}^*} = x^*(x) \in \mathbb{R}.$$

Let $A : \mathcal{X} \longrightarrow \mathcal{Y}$ be a continuous linear operator. As usual, $A^* : \mathcal{Y}^* \longrightarrow \mathcal{X}^*$ denotes its adjoint operator, that is, by using duality pairing notation, the linear operator such that

$$\langle Ax, y^*\rangle = \langle x, A^*y^*\rangle, \qquad \forall x \in \mathcal{X} \ \text{ and } \ \forall y^* \in \mathcal{Y}^*,$$

or equivalently, such that $y^*(Ax) = [A^*y^*](x)$. Moreover, it holds $\|A\| = \|A^*\|$ in each corresponding operator norm. We remark that the adjoint operator A^* is a map between the dual spaces $\mathcal{Y}^*$ and $\mathcal{X}^*$, that is, A^* maps linear operators into linear operators. This definition of adjoint operator in Banach spaces is the most general one, and the usual definition in an Hilbert setting is just a particular simplified case. Given a continuous and linear operator $A : \mathcal{H}_1 \longrightarrow \mathcal{H}_2$ between two Hilbert spaces $\mathcal{H}_1$ and $\mathcal{H}_2$, A^* is the Hermitian operator (or conjugate transpose operator, in finite dimensions) $A^* : \mathcal{H}_2 \longrightarrow \mathcal{H}_1$. Thanks to the isometric isomorphism based on the Riesz representation theorem [44], one can write $A^* : \mathcal{H}_2^* \cong \mathcal{H}_2 \longrightarrow \mathcal{H}_1^* \cong \mathcal{H}_1$, which falls under the scope of the previous general definition.

ETNA
Kent State University and
Johann Radon Institute (RICAM)

4.1. Duality mappings and the geometry of Banach spaces. The key tool for extending regularization methods to Banach spaces is the so-called duality map [2, 29, 36]. A duality map associates an element of a Banach space $\mathcal{X}$ to an element (or a subset of elements) of its dual $\mathcal{X}^*$. If $\mathcal{X}$ is a non-Hilbertian Banach space, $\mathcal{X}$ is not isometrically isomorphic to its dual $\mathcal{X}^*$, and the duality map is hence necessary. Formally, we have the following definition.

DEFINITION 4.1. *The (set-valued) mapping $J_r^{\mathcal{X}} : \mathcal{X} \longrightarrow 2^{\mathcal{X}^*}$, with $r > 1$, defined by*

$$J_r^{\mathcal{X}}(x) = \left\{ x^* \in \mathcal{X}^* : \langle x^*, x \rangle = \|x\| \|x^*\|, \|x^*\| = \|x\|^{r-1} \right\}, \quad \forall x \in \mathcal{X},$$

*is called **duality map** of $\mathcal{X}$ with gauge function $t \longmapsto t^{r-1}$.*

Duality mappings can be better understood by considering the subdifferential of the norm. We first recall that, given a (nonlinear) functional $f : \mathcal{X} \longrightarrow \mathbb{R} \cup \{+\infty\}$, then a linear functional $\tilde{x} \in \mathcal{X}^*$ is a subgradient of f at $x \in \mathcal{X}$ if and only if

$$f(z) \geq f(x) + \langle \tilde{x}, z - x \rangle, \quad \forall z \in \mathcal{X}. \tag{4.1}$$

The subdifferential of f is the set-valued map $\partial f : \mathcal{X} \longrightarrow 2^{\mathcal{X}^*}$ that associates an element $x \in \mathcal{X}$ with the set of all the subgradients of f at x, i.e. the set contained in $\mathcal{X}^*$, of linear functionals that satisfy (4.1). The subdifferential $\partial f(x)$ consists only of one element if and only if the functional f is differentiable at x, i.e. $\partial f(x) \in \mathcal{X}^*$ with a slight abuse of notation.

The classical Definition 4.1 lacks of practical intuition. The following important theorem links the concept of duality maps to the convex optimization tool of subdifferentials, giving a more simple and heuristic meaning to duality maps in terms of subdifferentials of the norm.

THEOREM 4.2 (see Asplund [3]). *Let $\mathcal{X}$ be a Banach space and $r > 1$. Then, the duality map $J_r^{\mathcal{X}}$ in Definition 4.1 is the subdifferential of the convex functional r-power norm of $\mathcal{X}$, that is,*

$$J_r^{\mathcal{X}}(x) = \partial \left(\frac{1}{r} \|\cdot\|^r \right)(x), \quad \forall x \in \mathcal{X}. \tag{4.2}$$

Asplund's Theorem suggests a practical way to compute duality maps, as the set of subgradients of the r-power of the norm, not evident from Definition 4.1.

We highlight that only in a Hilbert space $\mathcal{H}$ and only for $r = 2$, the duality map reduces to the identity operator, up to canonical isometric isomorphisms, so that with another slight abuse of notation we can write $J_2^{\mathcal{H}}(h) = \partial \left(\frac{1}{2} \|\cdot\|_{\mathcal{H}}^2 \right)(h) = h$ for all $h \in \mathcal{H}$. Moreover, by Definition 4.1, we notice that $\langle x^*, x \rangle = \|x\|^r$ for any $x^* \in J_r^{\mathcal{X}}(x)$, which is formally similar to the identity $\langle h, h \rangle = \|h\|^2$, involving the scalar product in a Hilbert space, for $r = 2$.

The duality map $J_r^{\mathcal{X}}$ is single-valued if and only if the Banach space $\mathcal{X}$ is smooth. Moreover, if $\mathcal{X}$ is also reflexive and strictly convex, then $\mathcal{X}^*$ is smooth and $J_r^{\mathcal{X}}$ is invertible [40]. In this case, its inverse map is given by $(J_r^{\mathcal{X}})^{-1} = J_{r^*}^{\mathcal{X}^*}$, where $J_{r^*}^{\mathcal{X}^*}$ is the duality map of the dual space $\mathcal{X}^*$ with gauge function $t \mapsto t^{r^*-1}$, being r^* the Hölder conjugate of r, that is, $\frac{1}{r} + \frac{1}{r^*} = 1$ or, equivalently, such that $r + r^* = r r^*$.

4.2. Dual spaces and duality maps of Lebesgue spaces L^p. In this work, we just consider the Lebesgue space $L^p(\Omega)$ of real functions, with $1 \leq p < +\infty$ and $\Omega \subseteq \mathbb{R}^n$ a measurable set. Recall that $L^p(\Omega)$ is the Banach space composed by all the measurable functions $x : \Omega \longrightarrow \mathbb{R}$ such that $\|x\|_p = \left(\int_\Omega |x(t)|^p \, dt \right)^{\frac{1}{p}} < +\infty$, where $\|x\|_p$ denotes its norm.

For $p > 1$, let $q > 1$ be its Hölder conjugate. The Hölder inequality for Lebesgue spaces states that, if $x_p \in L^p(\Omega)$ and $x_q \in L^q(\Omega)$, then the product function $x_p x_q$ is absolutely integrable, that is $x_p x_q \in L^1(\Omega)$, and $\|x_p x_q\|_1 \leq \|x_p\|_p \|x_q\|_q$. The special case $p = q = 2$

ETNA
Kent State University and
Johann Radon Institute (RICAM)

corresponds to the Cauchy-Schwarz inequality, being $L^2(\Omega)$ a Hilbert space with scalar product $\langle x, z\rangle = \int_\Omega x(t)z(t)\,dt$. The Hölder inequality is the key tool for proving that the norm of $L^p(\Omega)$ can be equivalently computed as

$$\|x\|_p = \sup_{g\in L^q(\Omega),\|g\|_q\leq 1} \int_\Omega |g(t)||x(t)|\,dt, \tag{4.3}$$

which allows to obtain many relations between $L^p(\Omega)$ and its dual space $(L^p(\Omega))^*$. Among them, the isometric isomorphism of $(L^p(\Omega))^*$ and $L^q(\Omega)$ is crucial in devising regularization algorithms [41]. More specifically, by basic functional analysis results, we know that for any linear functional $G \in (L^p(\Omega))^*$ there exists a unique function $g \in L^q(\Omega)$, called the "representative", such that

$$G(x) = \int_\Omega g(t)x(t)\,dt, \quad \forall x \in L^p(\Omega), \tag{4.4}$$

thus we can denote unambiguously G as G_g, with $g \in L^q(\Omega)$, and consider the injective mapping $G_g \in (L^p(\Omega))^* \longmapsto g \in L^q(\Omega)$. Notice that, thanks to (4.3),

$$\|G_g\|_{(L^p(\Omega))^*} = \sup_{x\in L^p(\Omega),\|x\|_p\leq 1} |G_g(x)| = \sup_{x\in L^p(\Omega),\|x\|_p\leq 1} \int_\Omega |g(t)||x(t)|\,dt = \|g\|_q, \tag{4.5}$$

so that the representative function g has finite norm if and only if the linear operator G_g is bounded, with equal corresponding norms. By the linearity of the integral w.r.t. the integrand, there exists an isometric isomorphism between $(L^p(\Omega))^*$ and $L^q(\Omega)$, for any $1 < p < +\infty$, referred to as canonical isomorphism. Thanks to it, we can implicitly identify any linear functional $G_g \in (L^p(\Omega))^*$ with its associated representative function $g \in L^q(\Omega)$.

The space $L^p(\Omega)$ is smooth if and only if $p > 1$, hence its duality map $J_r^{L^p(\Omega)}$ is a single-valued function for every $r \in (1, +\infty)$. By Asplund's Theorem 4.2, the duality map $J_r^{L^p(\Omega)} = J_r^p$ is directly computed. Thanks to the canonical isomorphism, it can be written as

$$J_r^p(x) = \|x\|_p^{r-p}|x|^{p-1}\,\mathrm{sign}(x) \in L^q(\Omega), \quad \forall x \in L^p(\Omega), \tag{4.6}$$

instead of $\langle J_r^p(x), h\rangle = \int_\Omega \|x\|_p^{r-p}|x(t)|^{p-1}\mathrm{sign}(x(t))h(t)dt$, so that $J_r^p(x) = G_g \in (L^p(\Omega))^*$ is written by means of its representative $g = \|x\|_p^{r-p}|x|^{p-1}\,\mathrm{sign}(x) \in L^q(\Omega)$, according to (4.4), with an implicit use of the canonical isometric isomorphism (4.5). In particular, in the Hilbert space $L^2(\Omega)$, equation (4.6) shows that J_2^2 reduces to the identity operator. We remark that the key parameter of J_r^p is p, which identifies the specific Banach space L^p, whereas r, which identifies the power of the norm functional, acts basically as scaling factor for all the components.

The discrete analogue of $L^p(\Omega)$ is ℓ^p, the Banach space composed by all the real sequences $x : \mathbb{N} \longrightarrow \mathbb{R}$ such that $\|x\|_p^p = \sum_i |x_i|^p < +\infty$, where $\|x\|_p$ denotes its norm. The duality map of $x = (x_n)_{n\in\mathbb{N}} \in \ell^p$ with the gauge function $t \mapsto t^{r-1}$ is denoted again as $J_r^p(x)$, and by means of the corresponding isometric isomorphisms between $(\ell^p)^*$ and ℓ^q, it is written as

$$J_r^p(x) = \left(\|x\|_p^{r-p}|x_n|^{p-1}\,\mathrm{sign}(x_n)\right)_{n\in\mathbb{N}} \in \ell^q,$$

with a straightforward analogy with the continuous case (4.6) of $L^p(\Omega)$ [41].

4.3. The Bregman distance. It is known that the Bregman distance, due to the geometrical properties of Banach spaces, is more appropriate for measuring the distance between two elements x and z instead of more conventional norm distances like $\|x - z\|^r$; see

ETNA
Kent State University and
Johann Radon Institute (RICAM)

e.g., [11, 12, 27]. The Bregman distance from a point $x \in \mathcal{X}$ associated to a convex functional $f : \mathcal{X} \longrightarrow \mathbb{R}$ is defined as the difference between the functional evaluated at x and its linear approximation around x, as follows:

DEFINITION 4.3 (see [7]). *Let $f : \mathcal{X} \longrightarrow \mathbb{R}$ be a convex and differentiable functional on a Banach space $\mathcal{X}$. Then, the* ***Bregman distance*** *$\Delta_f : \mathcal{X} \times \mathcal{X} \longrightarrow \mathbb{R}$ of f between $x \in \mathcal{X}$ and $z \in \mathcal{X}$ is defined as*

$$\Delta_f(x, z) = f(z) - f(x) - f'(x)(z - x),$$

where $f'(x) : \mathcal{X} \longrightarrow \mathbb{R}$ is the differential of f at the point x.

The role of a Bregman distance is similar to the role of any metric. However, a Bregman distance does not satisfy, in general, the triangle inequality nor symmetry. Moreover, the Bregman distance is a generalization of the classical square norm distance in Hilbertian contexts. Indeed, if $\mathcal{H}$ is a Hilbert space, then for $f(x) = \frac{1}{2}\|x\|^2_{\mathcal{H}}$, the Bregman distance Δ_f, now denoted as Δ_2, reduces to the conventional squared norm distance:

$$\Delta_2(x, z) = \frac{1}{2}\|x - z\|^2_{\mathcal{H}}.$$

This can be explicitly and straightforwardly computed in the Lebesgue space L^2.

In any Banach space $\mathcal{X}$, by virtue of Asplund's Theorem 4.2, the Bregman distance Δ_f for $f(x) = \frac{1}{r}\|x\|^r$ with $r > 1$, now denoted as Δ_r, can be written as

$$\Delta_r(x, z) = \frac{1}{r}\|x\|^r - \frac{1}{r}\|z\|^r - \langle J^{\mathcal{X}}_r(z), x - z\rangle, \quad \forall x, z \in \mathcal{X}, \tag{4.7}$$

where we implicitly consider a single-valued selection of $J^{\mathcal{X}}_r$. If $\mathcal{X}$ is smooth and uniformly convex, as L^p spaces with $p > 1$ where the iterative method in the next section is defined, for any x, y the Bregman distance $\Delta_r(x, y)$, with $r > 1$, is continuous, always nonnegative, and null if and only if $x = y$. In addition, $\lim_{n\to+\infty} \|x_n - x\| = 0$ if and only if $\lim_{n\to+\infty} \Delta_r(x, x_n) = 0$, which explains a kind of equivalence between Bregman and norm distances.

5. Iterative regularization in Banach spaces. In this section, we study iterative regularization algorithms in Banach spaces for the solution of the functional equation

$$Ax = y, \tag{5.1}$$

where $A : \mathcal{X} \longrightarrow \mathcal{Y}$ is a continuous and linear operator between two Banach spaces $\mathcal{X}$ and $\mathcal{Y}$, with given data $y \in \mathcal{Y}$ and unknown $x \in \mathcal{X}$. In particular, we consider the Landweber dual method [40] that is used in this paper to solve the FDEM inverse problem (3.4).

5.1. The Landweber method in Hilbert spaces. In this section, for the sake of simplicity, before discussing the iterative regularization in Banach spaces, we briefly start dealing with the basic Hilbertian case, that is, $\mathcal{X}$ and $\mathcal{Y}$ are both Hilbert spaces, which are always smooth and uniformly convex. By virtue of Riesz's theorem, which allows to identify a Hilbert space with its dual up to the canonical isometric isomorphisms as sketched in Section 4, the simplest iterative regularization algorithm for solving (5.1) is the descent method

$$x_{k+1} = x_k - \alpha_k \nabla f(x_k), \tag{5.2}$$

where $\alpha_k > 0$ is a proper step size. Scheme (5.2) is applied for the minimization of the least-squares *residual functional* $f : \mathcal{X} \longrightarrow \mathbb{R}$ defined as

$$f(x) = \frac{1}{2}\|Ax - y\|^2_{\mathcal{Y}}, \tag{5.3}$$

ETNA
Kent State University and
Johann Radon Institute (RICAM)

associated to the solution of the linear equation (5.1). The gradient $\nabla f(x_k) \in \mathcal{X}$ is the element such that $[\partial f(x_k)](x) = \langle \nabla f(x_k), x \rangle$, so that $\nabla f(x_k) \in \mathcal{X}$ is the representative of the (sub)differential $\partial f(x_k) \in \mathcal{X}^*$. We remark that, even if the function is smooth, we use the notation of the (sub)differential, since it allows us to distinguish between the (sub)differential, element of the dual space, and its representative element of the primal space. In addition, by a simple application of the chain rule to the (sub)differentiation of the 2-power residual (5.3), taking into account the subdifferential of the squared norm in Hilbert spaces, we have

$$\begin{aligned} \nabla f(x) &= \left(\left(\partial \left(\frac{1}{2} \| \cdot \|_{\mathcal{Y}}^2 \right) \Big|_{Ax-y} \right)^* \partial(Ax - y) \right)^* \\ &= ((Ax - y)^* A)^* = A^*(Ax - y), \end{aligned} \tag{5.4}$$

where the superscript * denotes the adjunction of linear operators, and the canonical isomorphism between X and X^* is implicitly used.

Iteration (5.2), when coupled to an efficient stopping criterion can be referred to as *implicit regularization*. In fact, the iteration number acts as a regularization parameter, according to the semi-convergence property [4], without any explicit regularization penalty term. Since the residual functional f is convex and differentiable, with $\nabla f(x_k) = A^*(Ax_k - y)$, (5.2) leads, for any initial guess $x_0 \in \mathcal{X}$ and fixed step length $\alpha_k \equiv \alpha \in (0, 2/\|A\|^2)$, to the well-known Landweber algorithm

$$x_{k+1} = x_k - \alpha A^*(Ax_k - y), \tag{5.5}$$

which guarantees convergence to the minimum norm least-square solution $\tilde{x} \perp N(A)$ for noiseless data [40]. Moreover, by considering the first-order condition $\nabla f(x_k) = 0$, that is, the normal equation $A^*Ax = A^*y$, the algorithm can be interpreted as a fixed point iterative method for the operator $P : \mathcal{X} \longrightarrow \mathcal{X}$ defined by $P(x) = x - \alpha(A^*(Ax - y))$ [9].

It is useful to notice that iteration (5.5) can be written as

$$\begin{aligned} x_{k+1} &= \arg\min_{x \in \mathcal{X}} \frac{1}{2} \|x - \big(x_k - \alpha \nabla f(x_k)\big)\|_{\mathcal{X}}^2 \\ &= \arg\min_{x \in \mathcal{X}} \left\{ \frac{1}{2} \|x - x_k\|_{\mathcal{X}}^2 + \alpha \langle \nabla f(x_k), x \rangle \right\}, \end{aligned} \tag{5.6}$$

where $\langle \cdot, \cdot \rangle$ denotes the scalar product of $\mathcal{X}$. The latter minimization problem is well defined, since the argument is coercive, being the sum of a quadratic functional and a linear one. Hence, since the two terms are convex and differentiable, by first order stationary conditions we have that (5.6) is equivalent to

$$\nabla \left(\frac{1}{2} \| \cdot - x_k \|_{\mathcal{X}}^2 + \alpha \langle \nabla f(x_k), \cdot \rangle \right) (x_{k+1}) = 0.$$

Formally, the minimization problem (5.6) can be recast in the framework of the theory of proximal operators [37]. Let us define, for a fixed $x' \in \mathcal{X}$ and a continuously differentiable functional g, the proximal operator $\operatorname{prox}_{\nabla g} : \mathcal{X} \longrightarrow \mathcal{X}$ as

$$\operatorname*{prox}_{\nabla g}(x') = \arg\min_{x \in \mathcal{X}} \left\{ \frac{1}{2} \|x - x'\|_{\mathcal{X}}^2 + \langle \nabla g(x'), x \rangle \right\}. \tag{5.7}$$

Then, the Landweber method (5.5) can be compactly written as

$$x_{k+1} = \operatorname*{prox}_{\alpha \nabla f}(x_k), \tag{5.8}$$

ETNA
Kent State University and
Johann Radon Institute (RICAM)

by virtue of (5.2) and (5.6). The scheme (5.8) heuristically shows that the iteration $x_{k+1} \in \mathcal{X}$ of (5.5) corresponds to the computation of a point which decreases $\langle \nabla f(x_k), x \rangle$ and simultaneously is close (i.e., proximal) to the previous iteration $x_k \in \mathcal{X}$. The step size α can be here thought of as a weight which balances between the two terms that are to be simultaneously decreased, $\frac{1}{2}\|x - x_k\|_{\mathcal{X}}^2$ and $\langle \nabla f(x_k), x \rangle$.

5.2. The Landweber method in Banach spaces. In [40], a generalization of the Landweber method to non-Hilbertian Banach spaces was first proposed under the hypothesis that $\mathcal{X}$ is smooth and uniformly convex. In the following, to simplify the notation, we will consider also $\mathcal{Y}$ to be a smooth Banach space. Such a generalization is not straightforward, because a Banach space is not necessarily isomorphic to its dual, so that the iteration formula (5.5) is not even formally consistent, since $A^* : \mathcal{Y}^* \longrightarrow \mathcal{X}^*$ cannot be applied to $Ax_k - y \in \mathcal{Y} \neq \mathcal{Y}^*$, as well as $x_k \in \mathcal{X}$ cannot summed to $\partial f(x_k) \in \mathcal{X}^* \neq \mathcal{X}$; see [9].

As already sketched in Section 4.1, the key tool for consistency are the so-called duality mappings, which allow generalizing the Landweber algorithm from Hilbert to Banach spaces. Indeed, $J_p^{\mathcal{Y}}(Ax_k - y) \in \mathcal{Y}^*$ can be an argument of the operator A^*, as well as $J_r^{\mathcal{X}}(x_k) \in \mathcal{X}^*$ can be summed to its result. On this formal ground, for fixed parameters $p, r > 1$, the Landweber iteration scheme for the solution of (5.1) in smooth, reflexive and strictly convex Banach spaces $\mathcal{X}$ and $\mathcal{Y}$ reads as

$$x_{k+1}^* = x_k{}^* - \alpha_k A^* J_p^{\mathcal{Y}}(Ax_k - y), \tag{5.9}$$

$$x_{k+1} = J_{r^*}^{\mathcal{X}^*}(x_{k+1}^*), \tag{5.10}$$

where $\alpha_k > 0$ is a proper variable step length and r^* is the Hölder conjugate of r [40]. Chosen an initial guess $x_0 \in \mathcal{X}$ (e.g., the null vector $x_0 = 0 \in \mathcal{X}$), the iteration starts with $x_0^* = J_r^{\mathcal{X}}(x_0) \in \mathcal{X}^*$. Since $x_k{}^* = J_r^{\mathcal{X}}(x_k)$, the scheme (5.9)–(5.10) can be also written as a single equation as follows

$$x_{k+1} = J_{r^*}^{\mathcal{X}^*}\left(J_r^{\mathcal{X}}(x_k) - \alpha_k A^* J_p^{\mathcal{Y}}(Ax_k - y)\right). \tag{5.11}$$

By analogy, we notice that the descent step of the Hilbertian method (5.5) is now performed in the dual space $\mathcal{X}^*$, since both $x_k{}^*$ and $A^* J_p^{\mathcal{Y}}(Ax_k - y)$ of (5.9) belong to $\mathcal{X}^*$. Hence, this algorithm is also referred to as Landweber dual method for the minimization of the p-power residual functional

$$f(x) = \frac{1}{p}\|Ax - y\|_{\mathcal{Y}}^p. \tag{5.12}$$

It is worth noting that, similarly to (5.4),

$$\begin{aligned} \partial f(x) &= \left(\left(\partial\left(\frac{1}{p}\|\cdot\|_{\mathcal{Y}}^p\right)\Big|_{Ax-y}\right)^* \partial(Ax - y)\right)^* \\ &= \left(\left(J_p^{\mathcal{Y}}(Ax - y)\right)^* A\right)^* = A^* J_p^{\mathcal{Y}}(Ax - y), \end{aligned} \tag{5.13}$$

where now $\partial f : \mathcal{X} \to \mathcal{X}^*$ with $\partial f(x) \in \mathcal{X}^*$ is not isometrically isomorphic to any element of the primal space $\mathcal{X}$, but it really is an element of the dual, hence the need of duality maps in the definition of (5.11). Moreover, this shows that the iterative step (5.9) is again a gradient method, now written as

$$x_{k+1}^* = x_k{}^* - \alpha_k \partial f(x_k)$$

ETNA
Kent State University and
Johann Radon Institute (RICAM)

and computed in the dual space $\mathcal{X}^*$, with a strong analogy with the iterative step (5.2) of the Hilbert setting, though computed in the primal space $\mathcal{X}$ in that case. Moreover, the role of the duality map $J_p^{\mathcal{Y}}$ in (5.9) is clear, as inner derivative of $\frac{1}{p}\|\cdot\|_{\mathcal{Y}}^p$ for the computation of $\partial f(x)$.

We report the following result of [5], which also explains the role of the duality map $J_{r^*}^{\mathcal{X}^*}$ of (5.10).

PROPOSITION 5.1 ([5]). *Let $\mathcal{X}$ and $\mathcal{Y}$ be two smooth, reflexive, and uniformly convex Banach spaces. Then, for $p, r > 1$, the Landweber iterative step (5.9) in Banach spaces*

$$x_{k+1} = J_{r^*}^{\mathcal{X}^*}\left({x_k}^* - \alpha_k A^* J_p^{\mathcal{Y}}(Ax_k - y)\right),$$

for the iterative solution of the ill-posed linear equation $Ax = y$, corresponds to the solution of the following minimization problem

$$x_{k+1} = \arg\min_{x\in\mathcal{X}} \left\{\Delta_r^{\mathcal{X}}(x, x_k) + \alpha_k \langle \partial f(x_k), x\rangle\right\}$$

where $f : \mathcal{X} \longrightarrow \mathbb{R}$ is the functional $f(x) = \frac{1}{p}\|Ax - y\|_{\mathcal{Y}}^p$ and $\Delta_r^{\mathcal{X}}$ denotes the Bregman distance (4.7) of $\mathcal{X}$.

Proof. Following (5.6), by using the Bregman distance $\Delta_r^{\mathcal{X}}$ of $\mathcal{X}$ instead of the norm distance, we can write

$$\begin{aligned} x_{k+1} &= \arg\min_{x\in\mathcal{X}} \left\{\Delta_r^{\mathcal{X}}(x, x_k) + \alpha_k \langle \partial f(x_k), x\rangle\right\} \\ &= \arg\min_{x\in\mathcal{X}} \left\{\frac{1}{r}\|x\|_{\mathcal{X}}^r + \frac{1}{r^*}\|x_k\|_{\mathcal{X}}^r - \left\langle J_r^{\mathcal{X}}(x_k), x\right\rangle + \alpha_k \left\langle \partial f(x_k), x\right\rangle\right\}. \end{aligned}$$

Since the functional to minimize is convex, differentiable, and coercive, the minimum point x_{k+1} is also a stationary point, hence

$$\partial\left(\frac{1}{r}\|\cdot\|_{\mathcal{X}}^r + \frac{1}{r^*}\|x_k\|_{\mathcal{X}}^r - \left\langle J_r^{\mathcal{X}}(x_k), \cdot\right\rangle + \alpha_k \left\langle \partial f(x_k), \cdot\right\rangle\right)(x_{k+1}) = 0.$$

By considering the Asplund equivalence (4.2) for the first term, since the second term is constant and the last two terms are linear, the latter equality leads to the following iterative gradient-type iteration

$$J_r^{\mathcal{X}}(x_{k+1}) - J_r^{\mathcal{X}}(x_k) + \alpha_k \partial f(x_k) = 0,$$

which can be written as

$$x_{k+1} = J_{r^*}^{\mathcal{X}^*}\left(J_r^{\mathcal{X}}(x_k) - \alpha_k \partial f(x_k)\right).$$

Taking into account (5.13) for $\partial f(x_k)$, this is exactly the Landweber dual method in a Banach space (5.11) for the minimization of the p-power residual functional (5.12). ∎

The previous proposition follows the rationale of (5.7), which shows that the Hilbert iteration (5.2) can be written as a *conventional* proximal step. Using the theory and rationales of Banach spaces, Proposition 5.1 allows us to write the Landweber iterative step (5.9)–(5.10) in Banach spaces as a proximal step with Bregman distance (4.7) as proximity measure in $\mathcal{X}$. More precisely, for a fixed $x' \in \mathcal{X}$ and given a continuously differentiable functional g, by defining the Bregman-proximal operator $\underset{\partial g}{\overset{\Delta_r^{\mathcal{X}}}{\operatorname{prox}}} : \mathcal{X} \longrightarrow \mathcal{X}$ as

$$\underset{\partial g}{\overset{\Delta_r^{\mathcal{X}}}{\operatorname{prox}}}(x') = \arg\min_{x\in\mathcal{X}} \left(\Delta_r^{\mathcal{X}}(x, x') + \langle \partial g(x'), x\rangle\right),$$

ETNA
Kent State University and
Johann Radon Institute (RICAM)

the basic iteration (5.9) reduces to

$$x_{k+1} = \operatorname*{prox}_{\alpha_k \partial f}^{\Delta_r^{\mathcal{X}}}(x_k),$$

which gives another useful interpretation of the Landweber dual algorithm in the context of convex optimization. As a final comment, we mention that in [9], the Landweber dual algorithm is shown to be a nonlinear version of well-known iterative projection algorithms for linear systems, such as the ART (Algebraic Reconstruction Technique) and DROP (Diagonally Relaxed Orthogonal Projection) methods [25].

6. Numerical tests. In this section, we study the accuracy of the regularization method of Section 5.2, namely, the dual Landweber method in Banach spaces, when recovering the electrical conductivity of the soil through the model (2.1), by solving (3.4). The goal of our numerical experiments is to illustrate the advantages deriving from a Banach space setting, in comparison to the numerical regularization methods used in [23] for the same problem of interest. In [23], the authors adopted the Truncated (Generalized) Singular Value Decomposition (T(G)SVD) as a regularization technique for (3.4). We refer the reader to [18, 19, 21, 23] for an overview of these methods applied to geophysical problems. In particular, as previously stated in Section 1, Banach spaces are known to better promote the presence of discontinuities in the sought solution, hence we expect to observe some improvements with respect to the TGSVD reconstructions of discontinuous distribution of the electrical conductivity. To this aim, we consider the following discontinuous piecewise signal as ground truth for the electrical conductivity of the soil

$$\sigma(z) = \begin{cases} 0.2, & z \in (0, 0.5), \\ 2, & z \in [0.5, 1.5], \\ 0.2, & z \in (1.5, \infty). \end{cases}$$

Then, using the notation of Section 3 we set $m = 20$ and $n = 500$. These values correspond to the following experimental set up: the measurements are collected at heights $h_i = \frac{2i}{m}$, for $i = 1, \ldots, m$, starting from the ground level up to 2 meters above the ground. The underground soil is discretized in the interval $[0, \tau]$, with 0 corresponding to the ground level and τ to the underground level at depth $\tau\rho$ (where ρ is the intercoil distance measured in meters), as $\{z_k\}_{k=0}^{n}$ (i.e., $z_0 = 0$ and $z_n = \tau$), with $\tau = 30$ in our simulations. We sample the ground truth $\sigma(z)$ in a vector $\boldsymbol{\sigma} \in \mathbb{R}^n$, so that $\sigma_k = \sigma(z_k)$, and generate a synthetic data set for each collocation method described in Section 3 by computing the exact right-hand side $\mathbf{g} = F\boldsymbol{\sigma}$, where F is the coefficient matrix corresponding to each method. Then, we consider a low noise regime and add additive white Gaussian noise (AWGN), with standard deviation equal to 0.005 to the noise-free data $\mathbf{g}$. The generated noisy acquisitions are displayed by the blue curve in Figure 6.1. In orange, background signals are reported, as better clarified in the following Section 6.1.

As a first step, we compute the solution of the discretized inverse problem (3.4), obtained using the three collocation methods described, respectively, in Sections 3.1, 3.2, and 3.3, using the dual Landweber method and the TGSVD regularization.

The GSVD approach is based on the *generalized singular value decomposition* [26] of the matrix pair (A, L), in the form

$$A = U\Sigma_A Z^{-1}, \qquad L = V\Sigma_L Z^{-1},$$

where the matrices U and V are orthogonal, Σ_A and Σ_L are diagonal, and Z is square invertible. We have used as a regularization operator L the discrete approximation of the first derivative.

ETNA
Kent State University and
Johann Radon Institute (RICAM)

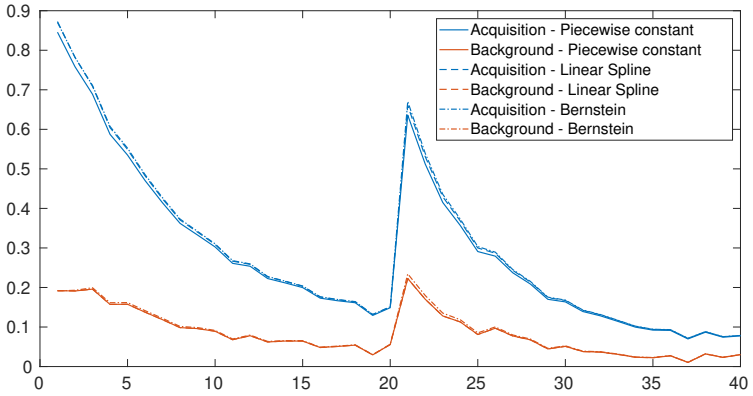

FIG. 6.1. *Acquired noisy signals (blue) and background signals (orange, see Section 6.1.) corresponding to the three collocations methods with an AWGN with standard deviation* 0.005.

The minimizer of the least-squares residual $\|F\mathbf{c} - \mathbf{g}\|_2$ (see system (3.4)), characterized by the minimal semi-norm $\|L\mathbf{c}\|_2$, is then expressed in terms of the factorization of A, and a regularized solution is obtained by truncating the representation to remove high-frequency components, corresponding to small diagonal entries of Σ_A; see [23] for details. In TGSVD, the truncation parameter plays the role of a regularization parameter. In our numerical tests, we choose the best possible value for it, i.e., the one which minimizes the 2-norm of the error. The aim is to show the best results that the method can produce.

For the Landweber method in Banach spaces, we have considered the Lebesgue spaces $\mathcal{Y} = L^p(\mathbb{R}^m)$ and $\mathcal{X} = L^p(\mathbb{R}^n)$ as acquisition and solution spaces, respectively, with $p = 1.3$ in both cases, and also as parameters of the duality mappings; see Section 6.4 for the choice of p. Hence, in this setting, the iterative scheme defined by (5.9) and (5.10) reads as

$$\mathbf{c}^*_{k+1} = \mathbf{c}^*_k - \alpha_k F^* J^p_p(F\mathbf{c}_k - \mathbf{g}), \qquad \mathbf{c}_{k+1} = J^{p^*}_{p^*}(\mathbf{c}^*_{k+1}).$$

The obtained results are reported in Figure 6.2. We observe that the Landweber method in Banach spaces estimates the height of the peak present in the signal significantly better than the TGSVD method. However, since working in Lebesgue spaces L^p with exponent p close to 1 enforces sparsity in the signal, we observe that the Landweber method is not able to reconstruct the non-zero constant background that is present in the conductivity ground truth signal. Indeed, after well approximating the peak, the reconstructed signals then go to zero in the deeper area of the inspected domain.

The previous test highlights the need of explicitly considering the background in the model. Hence, we propose to solve by the Landweber method the following minimization problem:

$$\bar{\mathbf{c}} = \arg\min_{\mathbf{c}\in L^p} \frac{1}{p}\|F(\mathbf{c} + \mathbf{b}) - \mathbf{g}\|^p_p\,, \tag{6.1}$$

where $\mathbf{b}$ is the background vector chosen as described in the next section. The final reconstructed signal is obtained as $\bar{\mathbf{c}} + \mathbf{b}$.

6.1. Landweber method in Banach spaces with background estimation. In our simulated setting, let us initially assume that the constant value of the background signal is exactly known to be 0.2. Hence, we repeat the previous test using a spatially constant background equal to the true value, that is, we set $\mathbf{b} = 0.2 \cdot (1, \ldots, 1)^T$.

ETNA
Kent State University and
Johann Radon Institute (RICAM)

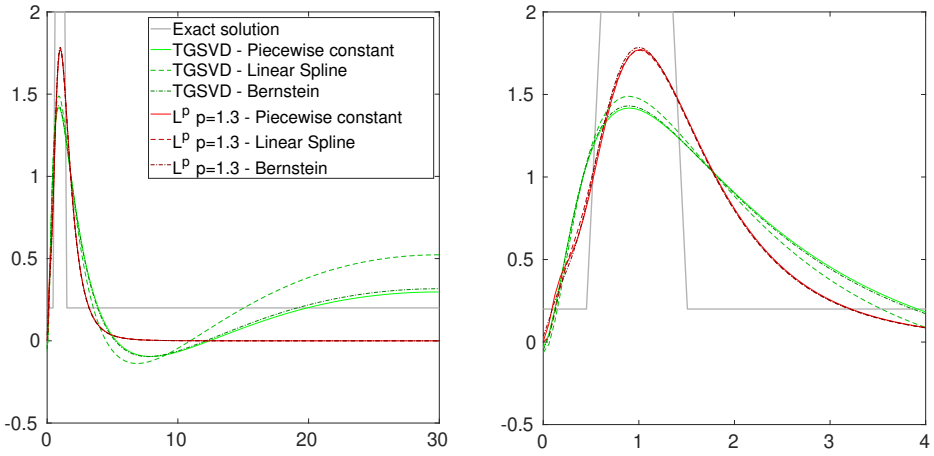

FIG. 6.2. *Reconstructions of the ground truth signal obtained with TGSVD regularization (green plots) and with Landweber method in L^p with $p = 1.3$ (red plots), with respect to the three considered collocations methods. On the left, plot of the signals on the whole interval $[0, \tau]$ with $\tau = 30$. On the right, zoom on the interval $[0, 4]$.*

The results are reported in Figure 6.3. It appears evident that the peak in the signal is better identified by the Banach Landweber method, which now also reaches a better accuracy in the reconstruction of the deep piecewise constant region, thanks to the introduction of the background in the model. However, the exact value of the background is usually not known. Hence, it is necessary to estimate it separately.

In order to obtain an estimate of the background to plug in (6.1), we assume to be able to obtain measurements taken in correspondence of regions where the soil conductivity is known to be constant. We point out here that the choice of constant values for the conductivity in every layer comes from the possible presence of very conductive materials in resistive mediums producing discontinuous distributions, which is present in real-world applications. In order to simulate the background measurements, given the background constant ground truth signal defined by $\sigma_b(z) = 0.2$, we repeat the same procedure described above to obtain measurements of the background, displayed in orange in Figure 6.1, for each collocation method described in Section 3: that is, we discretize σ_b as $\mathbf{b} = 0.2 \cdot (1, \dots, 1)^T$, and then for each collocation method we simulate the background measurements as $\mathbf{g_b} = F\mathbf{b}$, where F is the coefficient matrix corresponding to each method. Then, an estimate $\mathbf{b}^{\text{est}}$ of the background signal $\mathbf{b}$ is obtained using the TGSVD regularization method, in the three configurations presented, to solve $\mathbf{g_b} = F\mathbf{b}$. The results are shown in Figure 6.4.

To obtain an estimate of the ground truth conductivity signal, we apply the Landweber method in Banach spaces to (6.1), using the background $\mathbf{b}^{\text{est}}$ estimated in the previous step with the corresponding collocation method. We observe in Figure 6.5 that the estimation of the background does not compromise the accuracy of the Banach Landweber reconstructions, which are really similar to the previous ones of Figure 6.3 obtained using the exact background value.

The observation that some information on the background can improve the quality of numerical results is relevant from the applicative point of view. It should be kept in account when measuring data in the field. For example, when detecting the presence of pollutants in agricultural land, EMI measurements should be repeated in a soil presumed free of pollution to obtain an estimate of the background conductivity.

ETNA
Kent State University and
Johann Radon Institute (RICAM)

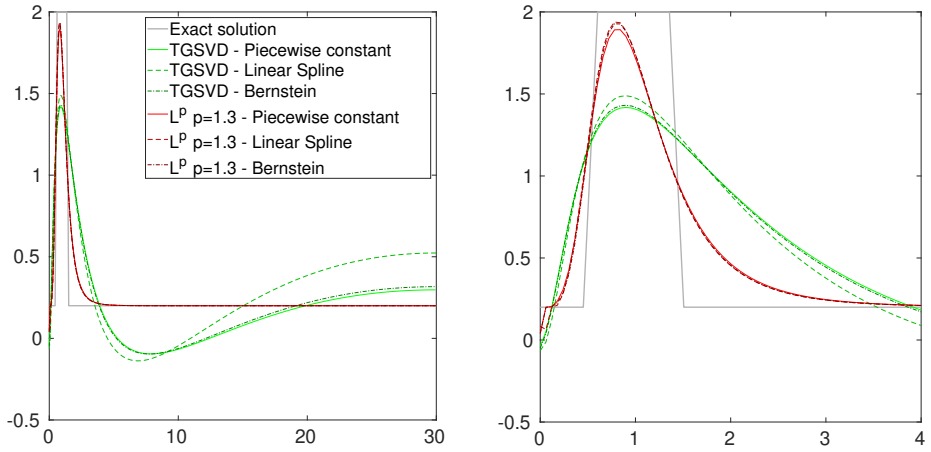

FIG. 6.3. *Reconstructions of the ground truth signal obtained by TGSVD regularization (green plots) and by the Landweber method in L^p with $p = 1.3$ (red plots), with background estimated as $\mathbf{b} = 0.2 \cdot (1, \dots, 1)^T$, with respect to the three collocations methods considered. On the left, plot of the signals on the whole interval $[0, \tau]$ with $\tau = 30$. On the right, zoom on the interval $[0, 4]$.*

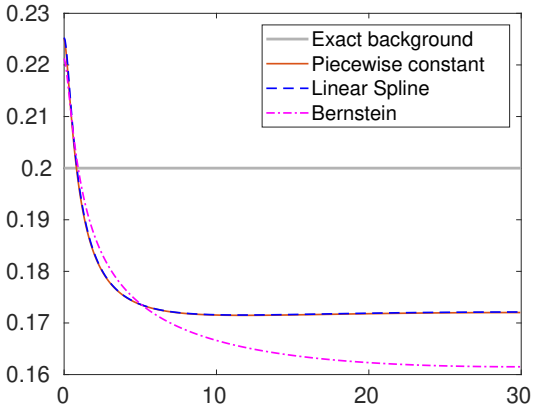

FIG. 6.4. *Reconstruction of the background signal obtained by TGSVD regularization methods with respect to the three collocation methods considered.*

6.2. Landweber method in Lebesgue spaces with variable exponent. We now consider as Banach spaces the unconventional Lebesgue spaces $L^{p(\cdot)}$ with variable exponent, thoroughly studied in [14, 24]. These spaces, as the name suggests, are defined in terms of a spatially variable exponent, that is point-wise varying. They are particularly suited to enforce spatially variant regularization thanks to the intrinsic flexibility given by the variable exponent. Here, we consider $\mathcal{X} = L^{p_{\mathcal{X}}(\cdot)}(\mathbb{R}^n)$ with variable exponent $p_{\mathcal{X}} = (p^k_{\mathcal{X}})_{k=1,\dots,n}$ as solution space and $\mathcal{Y} = L^{p_{\mathcal{Y}}(\cdot)}(\mathbb{R}^m)$ with variable exponent $p_{\mathcal{Y}} = (p^i_{\mathcal{Y}})_{i=1,\dots,m}$ as measurement space. The variable exponent $p_{\mathcal{Y}}$ is obtained by linearly interpolating the acquired data $\mathbf{g}$ between $(p_{\mathcal{Y}})_- = 1.1$ and $(p_{\mathcal{Y}})_+ = 1.4$, whilst the exponent $p_{\mathcal{X}}$ is obtained with linear interpolation between $(p_{\mathcal{X}})_- = 1.1$ and $(p_{\mathcal{X}})_+ = 1.4$ of the back-projected measured data $F^*\mathbf{g}$. For further details on the variable exponent selection, we refer the reader to [1, 31].

ETNA
Kent State University and
Johann Radon Institute (RICAM)

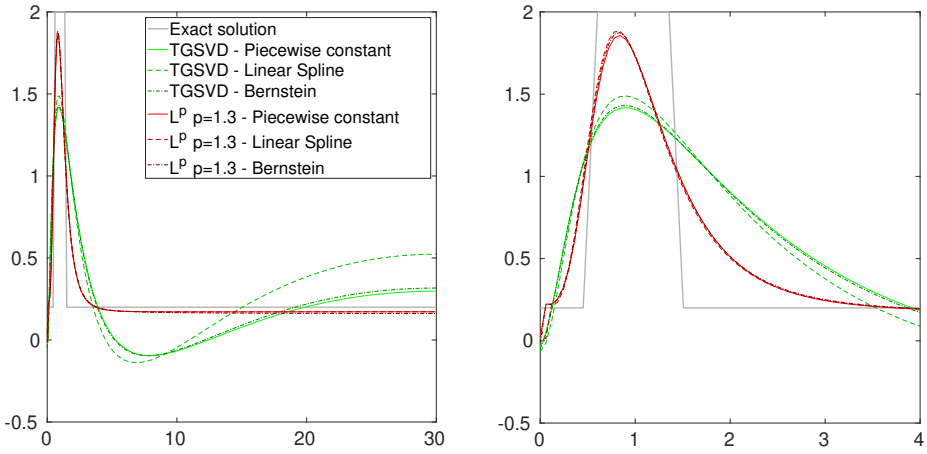

FIG. 6.5. *Reconstructions of the ground truth signal obtained by TGSVD regularization (green plots) and by the Landweber method in L^p with $p = 1.3$ (red plots), with the background estimated as in Figure 6.4, with respect to the three collocations methods considered. On the left, plot of the signals on the whole interval $[0, \tau]$ with $\tau = 30$. On the right, zoom on the interval $[0, 4]$.*

Due to the special definition of variable exponent Lebesgue spaces, the Landweber method in Banach spaces cannot be directly applied but requires a different definition in terms of the modular functions, for which we refer to [32, 33]. This new version of the Landweber method, however, coincides exactly with the Landweber method in Banach spaces in the case of a constant exponent. It can be seen as a generalization of the conventional method to the more general setting of modular spaces.

In Figure 6.6, we compare the reconstructed signals obtained in *classical* Lebesgue spaces with a constant exponent (red plots) and in variable exponent Lebesgue spaces (blue plots). We observe that all the reconstructions are more precise and accurate than the one obtained by TGSVD, displayed in green in Figure 6.5. Moreover, the choice of a variable exponent is further improving the reconstruction of the peak, without requiring heavier computations.

6.3. Robustness with respect to increasing noise in the signal. It is natural to wonder if the previous discussed regularization methods are robust with respect to different noise intensities, and, in particular, with respect to increasing noise.

We consider here the same ground truth signal as before, and we simulate three different noisy acquisitions with AWGN with standard deviation 0.01 (low noise regime), 0.02 (medium noise regime), and 0.04 (high noise regime). Then, we reconstruct the signal by TGSVD, by the Landweber method in L^p with $p = 1.3$ with background estimation, and by modular-based Landweber method [31] in variable exponent Lebesgue spaces $L^{p(\cdot)}$ with background estimation, with respect to the three considered collocations. Variable exponents are chosen as described in the previous section.

In Figure 6.7, we report all the attained reconstructions. In the considered low noise regime, we notice that the Landweber method in Banach spaces yields significantly better reconstructions than TGSVD, with a more noticeable peak and a more precise reconstruction of the background signal in the deeper part of the inspected domain. This behavior is more accentuated using a variable exponent (blue plots) rather than a constant one in Lebesgue spaces. However, with TGSVD it is still possible to clearly distinguish the peak in the

ETNA
Kent State University and
Johann Radon Institute (RICAM)

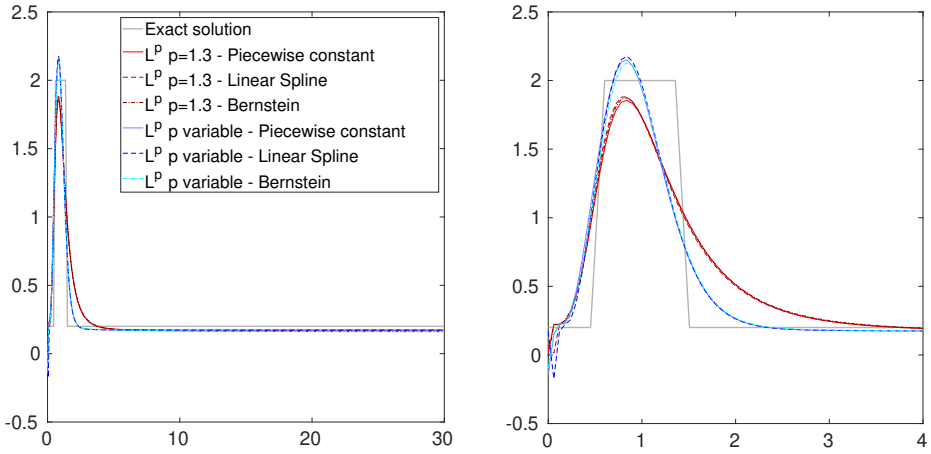

FIG. 6.6. *Reconstructions of the ground truth signal obtained in classical L^p with constant exponent $p = 1.3$ (red plots) and in Lebesgue spaces $L^{p(\cdot)}$ with variable exponent (blue plots). In both cases, the background is estimated as in Figure 6.4, with respect to the three considered collocations methods. On the left, plot of the signals on the whole interval $[0, \tau]$ with $\tau = 30$. On the right, zoom on the interval $[0, 4]$.*

conductivity profile. We remark that the behaviour of TGSVD on such test problems has already been observed in [23] for smaller noise levels.

With a medium noise regime, the TGSVD reconstructions are less accurate (piecewise constant-Bernstein) or not accurate at all (linear spline). Similarly, reconstructions provided by the Landweber method in L^p with a constant exponent $p = 1.3$ are less precise than the ones in a low noise regime, and they are more similar to the ones given by TGSVD (piecewise constant-Bernstein). They still present a trustable estimate of the background in the deeper part of the domain. On the other hand, the reconstructions obtained with variable exponent Lebesgue spaces Landweber-type regularization are not affected by the increased noise level in the acquisition: the peak is clearly visible and the background well estimated.

In the high noise regime, we see that the TGSVD method is not able to produce accurate reconstructions of the conductivity profile, no matter the collocation used: the retrieved signals are very far from the ground truth. With the Landweber method in L^p with a constant exponent $p = 1.3$, the peak is still distinguishable from the background, but the accuracy is much worse than in the medium and low noise settings. Instead, using a variable exponent we obtain much more precise conductivity profile estimations, which do not get much worse increasing the noise. The use of a variable exponent makes the Landweber method quite robust with respect to increasing levels of noise in the data.

6.4. Choice of the exponent. In this section, we investigate the role of the chosen exponent in the accuracy of the reconstruction of conductivity profiles with the Landweber method in Banach spaces, namely, Lebesgue spaces L^p with a constant exponent p and variable exponent Lebesgue spaces $L^{p(\cdot)}$. We consider a low noise regime (AWGN with standard deviation 0.01) and compare the conductivity profile estimated by TGSVD regularization, by Landweber method in L^p with $p = 1.1$, $p = 1.2$, $p = 1.3$, and $p = 1.4$, and by modular-based Landweber method in variable exponent Lebesgue spaces with exponents between 1.1 and 1.4, selected as described in Section 6.2.

It is well known that values of the exponent close to 1 are especially well-suited to retrieve sparse solutions, edges, and discontinuities. Hence, we study the restored conductivity profiles

ETNA
Kent State University and
Johann Radon Institute (RICAM)

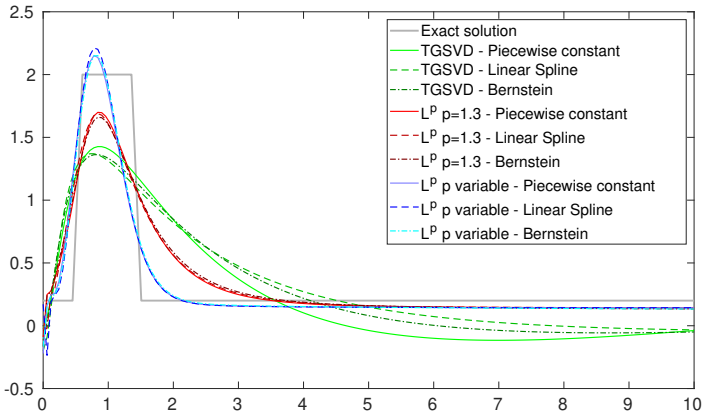

(a) Low noise regime: AWGN with standard deviation 0.01.

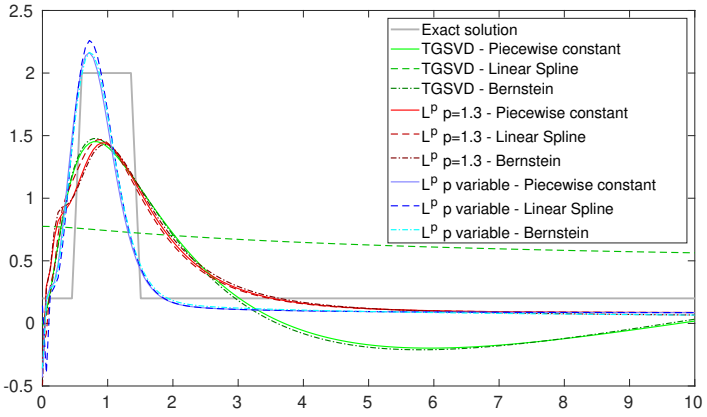

(b) Medium noise regime: AWGN with standard deviation 0.02.

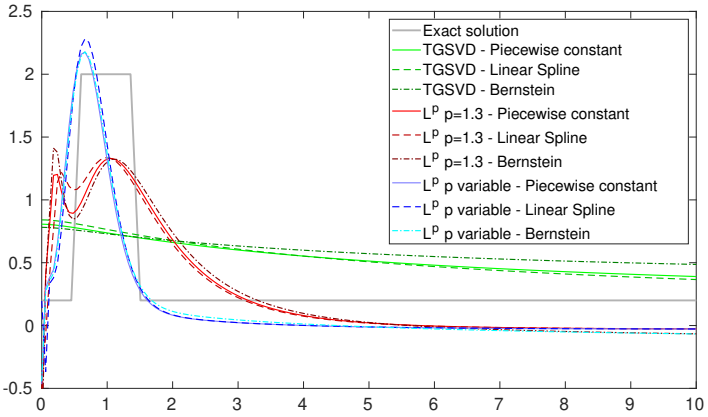

(c) High noise regime: AWGN with standard deviation 0.04.

FIG. 6.7. *Reconstructions of the ground truth signal obtained by TGSVD regularization (green plots) and by Landweber method in classical L^p with constant exponent $p = 1.3$ (red plots) and in Lebesgue spaces $L^{p(\cdot)}$ with variable exponent (blue plots), with respect to the three considered collocations methods. The background is estimated as in Figure 6.4. The plot is zoomed on the interval $[0, \tau]$ with $\tau = 10$.*

ETNA
Kent State University and
Johann Radon Institute (RICAM)

for the constant values $p = 1.1$, $p = 1.2$, $p = 1.3$, and $p = 1.4$, and with a variable exponent between 1.1 and 1.4. The rationale is that choosing an exponent close to 1 results in a better reconstruction of discontinuities and in a more enhanced peak. Thus, we expect to obtain a better reconstruction of the piecewise constant conductivity of the soil by choosing a smaller value for the constant exponent p.

As a first comment, we can see in Figure 6.7(a) (blue and green lines) and Figure 6.8 that all the Banach reconstructions result in better estimating the peak and the flat background in the deeper area of the inspected domain than the TGSVD ones.

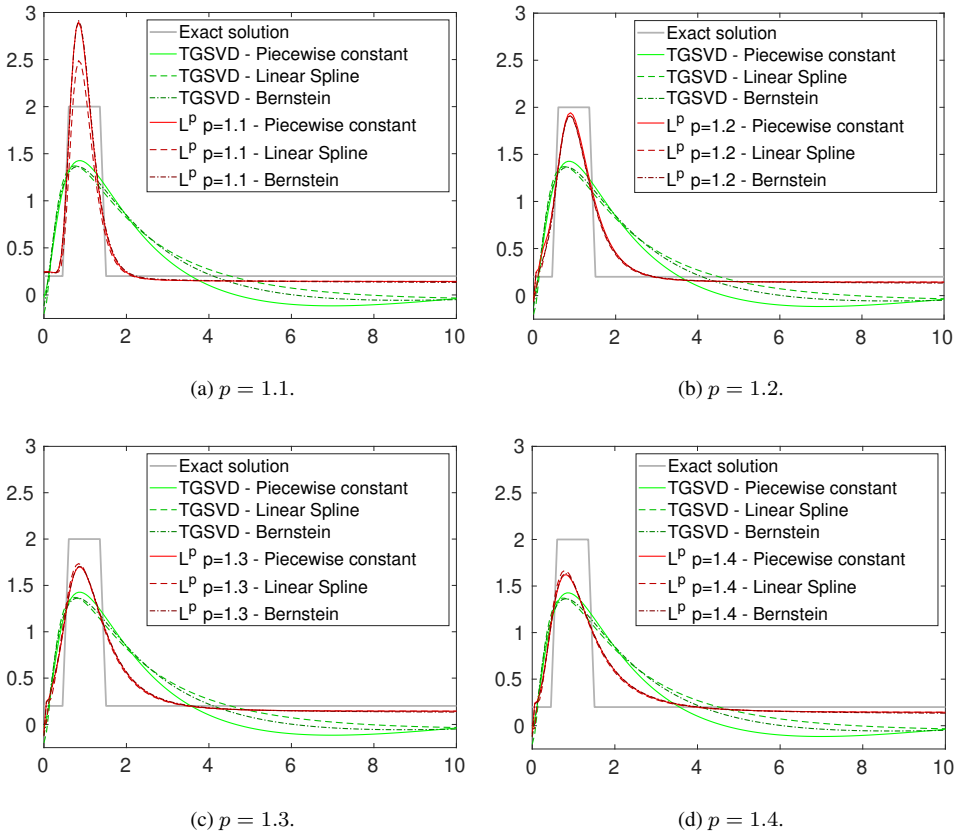

(a) $p = 1.1$. (b) $p = 1.2$.

(c) $p = 1.3$. (d) $p = 1.4$.

FIG. 6.8. *Results with various constant choices of the exponent.*

Regarding the behavior of the reconstructions with respect to the choice of the exponent, we observe in Figure 6.8 that the reconstruction of the background is good for all the exponent; in particular, in 0 it is better for 1.1, and it gets worse increasing the value of the exponent, because 0 is a value close to the discontinuity (hence, better retrieved by small exponents p). As for the peak, it is reconstructed fairly well for all the values and we notice that, for exponents closer to 1, the height of the peak increases making it more noticeable. One may think that an exponent $p \approx 1$ is a bad choice, since it leads to overestimated reconstruction of the peak. However, we remark that we are not so interested in estimating the exact point-wise values of the conductivity but more in understanding if there are discontinuities: this means that the reconstruction of the peak obtained with 1.1 is not necessarily worse than the one

ETNA
Kent State University and
Johann Radon Institute (RICAM)

obtained with 1.4. The best reconstruction attained with a constant value corresponds to $p = 1.2$. However, we observe in Figure 6.9 that the variable exponent estimation is visually more accurate than all the previous ones and does not require a precise tuning of the parameter.

In the variable exponent case, the reconstruction is very good (as for $p = 1.1$) but it presents some issues at 0, being the most difficult point where to estimate the conductivity, as it is at the border and also close to a discontinuity. The bad behavior at 0 is linked to the automatic selection of the variable exponent, which is based on the data. Indeed, the variable exponent is higher near the origin (because the signal is higher there), and this results in a worse reconstruction. This problem could be solved by choosing the variable exponent differently (manually), but an automatic selection leads to an overall good reconstruction without requiring heavy tuning, hence it is preferred.

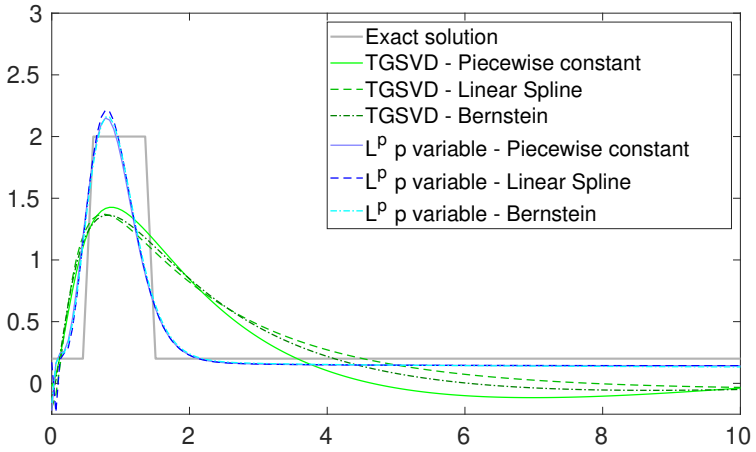

FIG. 6.9. *Results with a variable exponent $p(\cdot)$ between 1.1 and 1.4.*

We conclude the numerical section with a comment regarding the influence of the discretization scheme on the numerical results. We observe that there are not big differences in their performance. Linear splines produce the worst results for TGSVD in Figures 6.2, 6.3, and 6.5, while Bernstein polynomials are less effective than the other two approaches in approximating the background signal in Figure 6.4. The three approaches are more or less equivalent when the Landweber method in Banach spaces is employed, with the possible exception of Figure 6.8(a), where the linear spline interpolation reconstruction presents a peak whose height is significantly closer to the real amplitude of the solution. No particular differences are observed for a variable choice of the exponent. Concluding, the piecewise constant approximation appears to be the more convenient discretization scheme for the discontinuous solutions considered in our experimentation, since it gives good results and is the simpler to implement.

7. Conclusions. In this paper we proposed an iterative regularization method in Banach spaces for the inversion of a linear model for FDEM data. The method is based on the so-called dual Landweber method. Numerical experiments highlight the advantages of the proposed numerical approach when discontinuities are present in the solution. An experimental procedure for estimating the background signal and improve the accuracy of the result is also proposed. Future research will focus on extending the results of this paper to the nonlinear case and exploring higher-dimensional problems.

ETNA
Kent State University and
Johann Radon Institute (RICAM)

Acknowledgements. The authors are members of the GNCS group of INdAM and are partially supported by INdAM-GNCS 2024 Project "Algebra lineare numerica per problemi di grandi dimensioni: aspetti teorici e applicazioni" (CUP_E53C23001670001). PDA gratefully acknowledges Fondo Sociale Europeo REACT EU - Programma Operativo Nazionale Ricerca e Innovazione 2014-2020 and Ministero dell'Università e della Ricerca for the financial support. The research of CE, ML, GR is partially supported by the PRIN 2022 project "Inverse Problems in the Imaging Sciences (IPIS)" (2022ANC8HL). GR acknowledges partial support from Fondazione di Sardegna project "Computational Methods and Networks in Civil Engineering (COMANCHE)", and by the PRIN-PNRR 2022 project "AQuAInt - Approximation and Quadrature for Applicative Integral Models" (P20229RMLB). The research by CE and ML was supported in part by the MIUR Excellence Department Project awarded to Dipartimento di Matematica, Università di Genova, CUP D33C23001110001.

REFERENCES

[1] M. ALPARONE, F. NUNZIATA, C. ESTATICO, F. LENTI, AND M. MIGLIACCIO, *An adaptive L^p-penalization method to enhance the spatial resolution of microwave radiometer measurements*, IEEE Trans. Geosci. Remote Sens., 57 (2019), pp. 6782–6791.

[2] E. ASPLUND, *Positivity of duality mappings*, Bull. Amer. Math. Soc., 73 (1967), pp. 200–203.

[3] ———, *Fréchet differentiability of convex functions*, Acta Math., 121 (1968), pp. 31–47.

[4] M. BERTERO AND P. BOCCACCI, *Introduction to Inverse Problems in Imaging*, Institute of Physics Publishing, Bristol, 1998.

[5] B. BONINO, C. ESTATICO, AND M. LAZZARETTI, *Dual descent regularization algorithms in variable exponent Lebesgue spaces for imaging*, Numer. Algorithms, 92 (2023), pp. 149–182.

[6] K. BREDIES, *A forward-backward splitting algorithm for the minimization of non-smooth convex functionals in Banach space*, Inverse Problems, 25 (2008), Paper No. 015005, 20 pages.

[7] L. M. BRÈGMAN, *A relaxation method of finding the common points of convex sets and its application to the solution of problems in convex programming*, Ž. Vyčisl. Mat i Mat. Fiz., 7 (1967), pp. 620–631.

[8] H. BREZIS, *Functional Analysis, Sobolev Spaces and Partial Differential Equations*, Springer, New York, 2011.

[9] P. BRIANZI, F. DI BENEDETTO, AND C. ESTATICO, *Preconditioned iterative regularization in Banach spaces*, Comput. Optim. Appl., 54 (2013), pp. 263–282.

[10] A. BUCCINI AND P. DÍAZ DE ALBA, *A variational non-linear constrained model for the inversion of FDEM data*, Inverse Problems, 38 (2022), Paper No. 014001, 21 pages.

[11] M. BURGER AND S. OSHER, *Convergence rates of convex variational regularization*, Inverse Problems, 20 (2004), pp. 1411–1421.

[12] D. BUTNARIU AND E. RESMERITA, *Bregman distances, totally convex functions and a method for solving operator equations in Banach spaces*, Abstr. Appl. Anal., 2006 (2006), Paper No. 84919, 39 pages.

[13] I. CIORANESCU, *Geometry of Banach spaces, Duality Mappings and Nonlinear Problems*, Kluwer, Dordrecht, 1990.

[14] D. V. CRUZ-URIBE AND A. FIORENZA, *Variable Lebesgue Spaces: Foundations and Harmonic Analysis*, Birkhäuser/Springer, Heidelberg, 2013.

[15] C. DE BOOR, *A Practical Guide to Splines*, Springer, New York, 1978.

[16] G. DEIDDA, P. DÍAZ DE ALBA, C. FENU, G. LOVICU, AND G. RODRIGUEZ, *FDEMtools: a MATLAB package for FDEM data inversion*, Numer. Algorithms, 84 (2020), pp. 1313–1327.

[17] G. P. DEIDDA, P. DÍAZ DE ALBA, F. PES, AND G. RODRIGUEZ, *Forward electromagnetic induction modelling in a multilayered half-space: an open-source software tool*, Remote Sensing, 15 (2023), Paper No. 1772, 36 pages.

[18] G. P. DEIDDA, P. DÍAZ DE ALBA, AND G. RODRIGUEZ, *Identifying the magnetic permeability in multi-frequency EM data inversion*, Electron. Trans. Numer. Anal., 47 (2017), pp. 1–17. https://etna.ricam.oeaw.ac.at/vol.47.2017/pp1-17.dir/pp1-17.pdf.

[19] G. P. DEIDDA, P. DÍAZ DE ALBA, G. RODRIGUEZ, AND G. VIGNOLI, *Smooth and sparse inversion of EMI data from multi-configuration measurements*, in 2018 IEEE 4th International Forum on Research and Technology for Society and Industry (RTSI) (RTSI 2018), Palermo, Italy, IEEE Conference Proceedings, Los Alamitos, 2018, pp. 1–6.

[20] ———, *Inversion of multiconfiguration complex EMI data with minimum gradient support regularization: a case study*, Math. Geosci., 52 (2020), pp. 945–970.

ETNA
Kent State University and
Johann Radon Institute (RICAM)

[21] G. P. DEIDDA, C. FENU, AND G. RODRIGUEZ, *Regularized solution of a nonlinear problem in electromagnetic sounding*, Inverse Problems, 30 (2014), Paper No. 125014, 27 pages.
[22] P. DÍAZ DE ALBA, L. FERMO, F. PES, AND G. RODRIGUEZ, *Regularized minimal-norm solution of an overdetermined system of first kind integral equations*, Numer. Algorithms, 92 (2023), pp. 471–502.
[23] P. DÍAZ DE ALBA, L. FERMO, C. VAN DER MEE, AND G. RODRIGUEZ, *Recovering the electrical conductivity of the soil via a linear integral model*, J. Comput. Appl. Math., 352 (2019), pp. 132–145.
[24] L. DIENING, P. HARJULEHTO, P. HÄSTÖ, AND M. RUZICKA, *Lebesgue and Sobolev Spaces with Variable Exponents*, Springer, Berlin, Heidelberg, 2011.
[25] T. ELFVING, T. NIKAZAD, AND P. C. HANSEN, *Semi-convergence and relaxation parameters for a class of SIRT algorithms*, Electron. Trans. Numer. Anal., 37 (2010), pp. 321–336. https://etna.ricam.oeaw.ac.at/vol.37.2010/pp321-336.dir/pp321-336.pdf.
[26] G. H. GOLUB AND C. F. VAN LOAN, *Matrix Computations*, 3rd ed., Johns Hopkins University Press, Baltimore, 1996.
[27] M. GRASMAIR, *Generalized Bregman distances and convergence rates for non-convex regularization methods*, Inverse Problems, 26 (2010), Paper No. 115014, 16 pages.
[28] J. HADAMARD, *Lectures on Cauchy's problem in linear partial differential equations*, Dover, New York, 1953.
[29] B. T. KIEN, *The normalized duality mapping and two related characteristic properties of a uniformly convex Banach space*, Acta Math. Vietnam., 27 (2002), pp. 53–67.
[30] R. KRESS, *Numerical Analysis*, Springer, New York, 1998.
[31] M. LAZZARETTI, *Optimisation Algorithms in Non-Standard Banach Spaces for Inverse Problems in Imaging*, PhD. Thesis, Université Côte d'Azur; Università di Genova, Genova, 2024.
[32] M. LAZZARETTI, L. CALATRONI, AND C. ESTATICO, *Modular-proximal gradient algorithms in variable exponent Lebesgue spaces*, SIAM J. Sci. Comput., 44 (2022), pp. A3463–A3489.
[33] M. LAZZARETTI, Z. KERETA, C. ESTATICO, AND L. CALATRONI, *Stochastic gradient descent for linear inverse problems in variable exponent Lebesgue spaces*, in Scale Space and Variational Methods in Computer Vision SSVM 2023, L. Calatroni, M. Donatelli, S. Morigi, M. Prato, M. Santacesaria, eds., Springer, Cham, 2023, pp. 457–470.
[34] J. LINDENSTRAUSS AND L. TZAFRIRI, *Classical Banach Spaces*, Springer, Berlin, 1973.
[35] J. D. MCNEILL, *Electromagnetic terrain conductivity measurement at low induction numbers*, Technical Note TN-6, Geonics Limited, 1980.
[36] P. M. MILIČIĆ, *On moduli of expansion of the duality mapping of smooth Banach spaces*, JIPAM. J. Inequal. Pure Appl. Math., 3 (2002), Paper No. 55, 7 pages.
[37] N. PARIKH AND S. BOYD, *Proximal algorithms*, Found. Trends Optim., 1 (2014), pp. 123–231.
[38] F. PES AND G. RODRIGUEZ, *The minimal-norm Gauss-Newton method and some of its regularized variants*, Electron. Trans. Numer. Anal., 53 (2020), pp. 459–480. https://etna.ricam.oeaw.ac.at//vol.53.2020/pp459-480.dir/pp459-480.pdf.
[39] ———, *A doubly relaxed minimal-norm Gauss–Newton method for underdetermined nonlinear least-squares problems*, Appl. Numer. Math., 171 (2022), pp. 233–248.
[40] F. SCHÖPFER, A. K. LOUIS, AND T. SCHUSTER, *Nonlinear iterative methods for linear ill-posed problems in Banach spaces*, Inverse Problems, 22 (2006), pp. 311–329.
[41] T. SCHUSTER, B. KALTENBACHER, B. HOFMANN, AND K. S. KAZIMIERSKI, *Regularization Methods in Banach Spaces*, de Gruyter, Berlin, 2012.
[42] M. UNSER AND S. AZIZNEJAD, *Convex optimization in sums of Banach spaces*, Appl. Comput. Harmon. Anal., 56 (2022), pp. 1–25.
[43] Y. XU, *Sparse machine learning in Banach spaces*, Appl. Numer. Math., 187 (2023), pp. 138–157.
[44] K. YOSIDA, *Functional Analysis*, Springer, 1970.